

Determination of Electron Density and Nebula Mass for NGC 6210

T. Harvey (29974232)

School of Physics & Astronomy, University of Southampton, UK, SO17 1BJ

1 Abstract

Observations of the planetary nebula NGC 6210, taken in April 2019 using the IAC-80 and the CAMELOT CCD, have been used to determine the mass of the nebula. Narrowband observations of the forbidden [SII] doublet are used to estimate the electron density of the nebula, which is found to be $3600 \pm 1600 \text{ cm}^{-3}$. Narrowband images of line and continuum emission of H β and H α , along with the corresponding B and V broadband data, have been used to calibrate the observations to obtain absolute flux density for the lines, which was found to be $(4.14 \pm 0.01) \times 10^{-10} \text{ erg cm}^{-2} \text{ s}^{-1}$ for H α and $(1.14 \pm 0.03) \times 10^{-10} \text{ erg cm}^{-2} \text{ s}^{-1}$ for the H β flux density. This H β flux density is comparable to measurements in literature, but it is likely that the H α flux density is overestimated due to a poor calibration. Using the H β flux density, and the electron density, the total ionised mass of the planetary nebulae was found to be $0.071 \pm 0.047 M_{\odot}$, which is formally consistent with the value of $0.07 M_{\odot}$ given in literature. This paper demonstrates the ability to estimate line ratios, and indeed absolute fluxes, using only narrowband imaging when a spectrometer is not available. Although the observed mass is consistent with the literature, it is likely an underestimate of the true mass, as much of the mass is likely to be contained in a low density, low surface brightness halo that is not detectable in these observations.

2 Introduction

Planetary nebulae (PNe) are expanding shells of ionised gas that are ejected from stars at the end of their lives. They are a type of emission nebulae, and are thought to be relatively short lived (around 10^5 years), compared to other stages of a stellar life cycle (Nishiyama, 2018). NGC 6210 is an example of a bright, elliptical planetary nebula, located at RA(2000) $16^h 44^m 29.51^s$, Dec(2000) $+23^\circ 47' 59.49''$ (Gaia Collaboration, 2018). It is about $40''$ by $30''$, but the bright inner region, which is $10^4 \times$ brighter than the outside filaments, is only $13''$ by $16''$. The structure of the nebula can be seen in Figure 1, which is a false colour composite image of the nebula. It is at a distance of 1.67 ± 0.41 kpc, and is 1 kpc above the galactic plane, meaning that there is low interstellar extinction (See Bohigas et al., 2014 and references therein). It has a roughly uniform temperature of 9500K (Pottasch, S. R. et al., 2009).

Planetary nebulae are produced as stars between $1-8 M_{\odot}$ transition from asymptotic giant branch (AGB) stars to white dwarfs. Gas and dust is thrown off the AGB star at high velocity, which expands and cools, leaving behind a white dwarf surrounded by a shell of ionised gas. The white dwarf produces UV radiation which ionises the gas in the nebulae, causing the emission of a discrete line spectra (Pottasch, 1984). The presence of different lines, and their relative strengths, provide an insight into the composition and temperature of a planetary nebulae. PNe's emit almost entirely in these spectral lines, and do not have a significant continuum emission, although it is still necessary to perform a continuum subtraction when calibrating the acquired data.

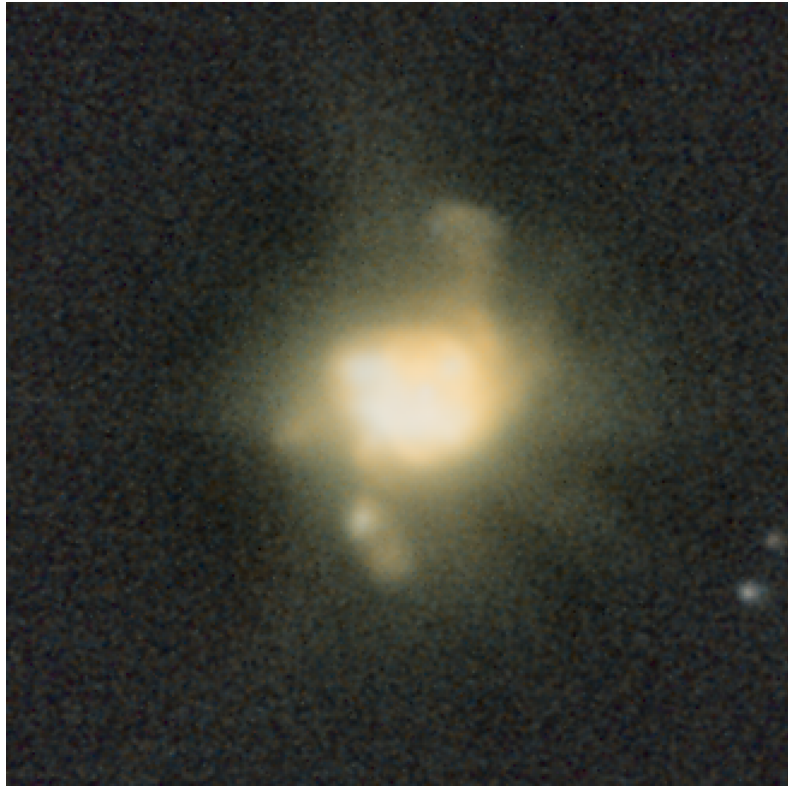


Figure 1: False colour composite picture of NGC 6210 using data from the IAC-80, made from narrowband H α , H β and SII images.

2.1 Theory

One of the most prominent lines in many stellar objects is Hydrogen Alpha, or H α , as hydrogen is the most abundant element in the universe, and hydrogen is ionised by the ultraviolet photons that are commonly emitted by the central star ($T_{\text{eff}} \approx 50,000K$). The freed electrons then collide with another hydrogen atom, and will deexcite down the excitation levels by emitting photons of equivalent energy to the difference in energy level. The most prominent of these energies is the Balmer series transition from n=3 to n=2, which produces a photon of wavelength 656.3 nm - this is H α . The less common transition is the Balmer series transition from n=4 to n=2, which produces a photon of 486.1nm - this is H β . The H β flux has some temperature dependence, as a higher thermal excitation is needed to populate the higher energy levels often enough to produce a measurable H β flux.

The other emission line used here is the [SII] doublet, [SII] (6716Å and 6731Å), which is proportional to N_e , the electron density of the nebula. The [SII] doublet comes from $^2D_{3/2} \rightarrow ^4S$ and the $^2D_{5/2} \rightarrow ^4S$ transitions for 6731Å and 6716Å respectively. These sulphur lines are known as forbidden lines, as they occur via spontaneous transmission, which has a very low probability of occurring. The wavelengths of the doublet, 6731Å and 6717Å are so close because the levels, shown above (5/2 and 3/2) have very similar energies. This means that a collision with enough energy to populate one of the energy levels will probably also populate the other, meaning they have a similar chance of being populated. There are other differences between the levels; the 5/2 level can hold 6 electrons, whereas the 3/2 level can only hold 4, and the 5/2 level has a lifetime of 3846 seconds, but the 3/2 level has a lifetime of 1136 seconds. In very low density gas, the time between collisions is long enough that most electrons have time to emit a forbidden photon before they are collisionally de-excited. So in the low density limit, the ratio of the line strengths is just 6/4, the ratio of the electrons in the 5/2 level to the 3/2 level. In dense environments it is much more likely that the electron will de-excite due to a collision before spontaneous transmissions occurs. In the high density limit, collisions are frequent and so the lifetime of the level is important - a shorter lifetime means a higher likelihood of photon emission. The SII ratio is given by the ratio of the lifetimes multiplied by the ratio of the number of electrons in each level, as more electrons still means more emission. This has been found to

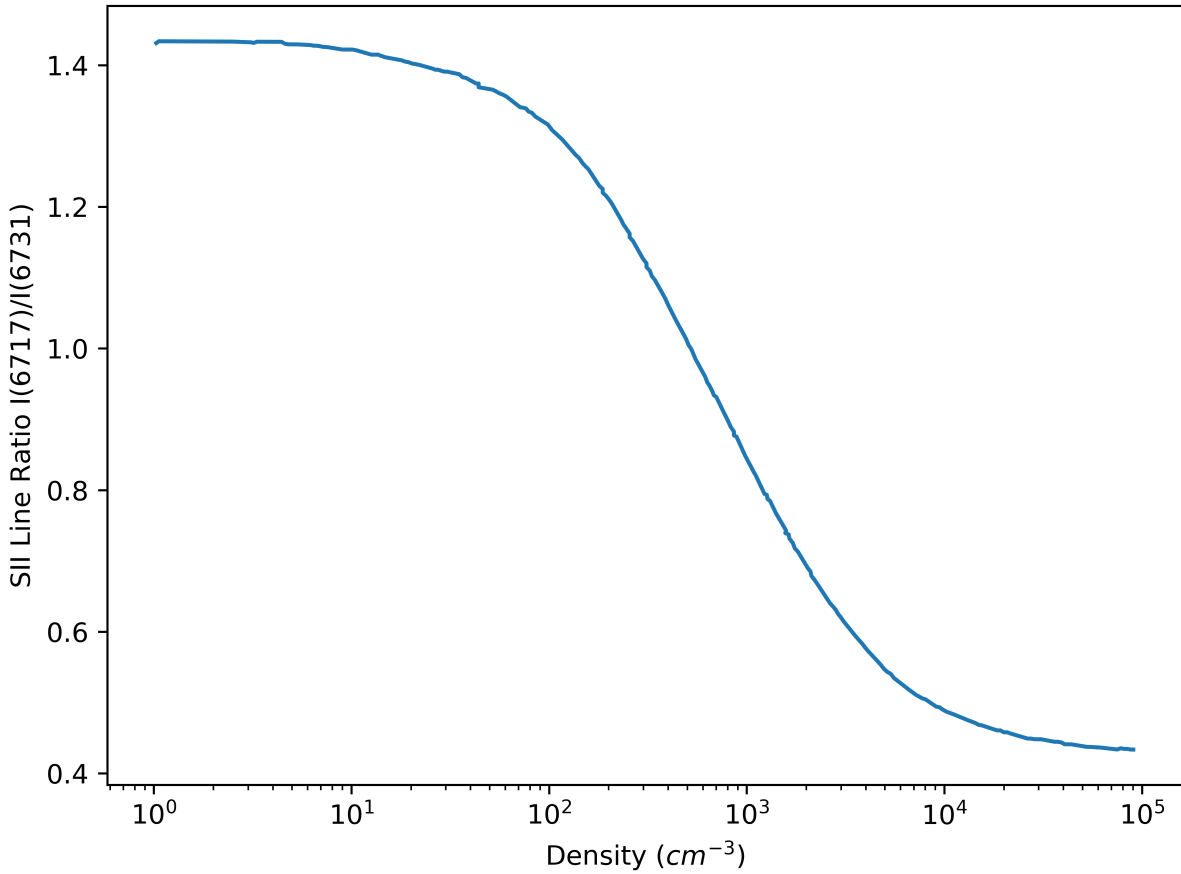


Figure 2: Figure showing the SII ratio vs the electron density. Data taken from Osterbrock and Ferland, 2006.

be around 0.44 at $10,000 \text{ cm}^{-3}$. In between these upper and lower limits, the ratio changes between these two values in a way that is proportional to the density - the lifetime and the number of electrons in each level have a different weight in the line density calculation that depends on the density of the gas (Information on ratios and levels taken from Osterbrock and Ferland, 2006). This is shown in Figure 2. This means that a measurement of the ratio between the two lines in the doublet can be used to estimate the mean electron density of the nebula. Other doublets, such as [CIII] and [OII] can also be used to determine densities, and [OIII] and [NII] can be used to determine temperatures, however data from those filters is not available for this object.

The mass of the nebula can be determined from the mean density of the nebula and the $\text{H}\beta$ flux density as follows. For the $n = 4$ hydrogen level, it can be written that $n_4 = n_e n_H f_4(T_e)$ where n_4 is the density of electrons in the 4th level, n_e is the electron number density, n_H is the proton number density, and $f_4(T_e)$ is a constant with a small temperature dependence. This can then be used to find the emission coefficient for $\text{H}\beta$, $j_{\text{H}\beta}$, which is

$$j_{\text{H}\beta} = n_4 A_{42} h v_{42} / 4\pi = n_e n_H f_4(T_e) A_{42} h v_{\beta} / 4\pi \quad (1)$$

where A_{42} is the Einstein coefficient for spontaneous transmission, which is a constant for the given atom and energy levels. v_{β} is the frequency of the $\text{H}\beta$ emission and the other constants have been defined previously. The constants $f_4(T_e) A_{42}$ are collected as $\alpha_{\text{H}\beta}^{\text{eff}}$, the effective $\text{H}\beta$ recombination coefficient, which for a nebula temp of 10,000K is found to be $3.03 \times 10^{-14} \text{ cm}^3 \text{ s}^{-1}$ (Irwin, 2007). The luminosity of the object in the $\text{H}\beta$ line is then the emission coefficient integrated over the volume of the nebula.

$$L_{\text{H}\beta} = \int_V 4\pi j_{\text{H}\beta} dV = \alpha_{\text{H}\beta}^{\text{eff}} h v_{\beta} \int_V n_e n_H dV \quad (2)$$

Date	Exposure Time(s)	Type	Filter	Number
07/04/19	30	Science	B	5
07/04/19	30	Science	V	5
07/04/19	30	Science	R	5
07/04/19	90	Science	n20Ha[NII]	5
07/04/19	600	Science	n27Hact	5
07/04/19	15	Science	Open	5
10/04/19	300	Science	n32[SII]	5
11/04/19	300	Science	n34[SII]	5
11/04/19	120	Science	n10Hb	5
11/04/19	100	Science	n1Hbred	5

Table 1: Table showing science data collected for NGC 6210, from the IAC-80 at the Observatorio del Teide in Tenerife.

This is of course also equal to the observed $H\beta$ flux integrated over the surface of the sphere centred on the nebula with radius equal to the distance to the nebula, d . I.e. $L_{H\beta} = 4\pi d^2 F_{H\beta}$. It is also trivial to see the total mass of the hydrogen (the dominant nebula component) will simply be $M = \int_V m_H n_H dV$ where n_H is the hydrogen number density and m_H is the mass of a hydrogen atom. The method to determine the mean electron density $\langle n_e \rangle$ has already been shown above, so equating the two expressions for the $H\beta$ luminosities and subbing in the expression for the mass it can be shown that

$$M = \frac{4\pi m_H d^2 F_{H\beta}}{\alpha_{H\beta} h v_\beta \langle n_e \rangle} \quad (3)$$

(Adapted from Bohigas et al., 2014) This expression is only an approximation, and the estimated masses will be incorrect if there is significant density inhomogeneity in the nebula.

3 Observations

The observations were taken in April 2019, at the Observatorio del Teide on Tenerife using the IAC-80 telescope. The observations taken, along with the exposure time, filter and number are shown in Table 1. The detector used was the CAMELOT CCD, which with 2148×2048 pixels, provides a field of view of about $10.5' \times 10.5'$. The science images were taken in a variety of filters, including both narrowband and wideband. The wideband filters were the standard Johnson-Bessell B, V and R filters, and the narrowband filters were the $H\alpha$, $H\alpha$ continuum, $H\beta$, $H\beta$ red and two SII filters. These narrowband filters were n20Ha[NII], n27Hact, n10Hb, n1Hbred, n32[SII] and n34[SII], and more information on them can be found on the SVO Filter Profile Service page for the IAC-80 (Rodrigo, 2020). These narrowband filters are very narrow, with widths below 50Å, and are designed to be on (on-band) or near (off-band) a particular emission lines. The continuum/red filters are designed to be very close to the line emission to measure the continuum flux so that with some calibration the flux that is purely from the emission line can be determined.

3.1 Data Reduction and Analysis

The raw data that is collected by the CCD must first be processed so it can be used to determine meaningful results. During the same week the other data was collected both bias and flat frames were also collected. Around 15 flat frames were taken for each filter, using a flat field panel on the inside of the dome, and 21 bias frames were also taken. The CAMELOT CCD does not require dark frames to be taken as it is cooled to around $-105^\circ C$, and so there is a negligible dark current.

Bias frames, which account for the count correction applied to the image by the detector, and for the readout noise of the CCD, were taken. They were used to create a master bias image by taking the mean value for each pixel in the frame, but using a sigma-clipping algorithm to clip outliers (above 5σ) between

the individual frames, to ensure the mean wasn't skewed. Using the mean instead of the median lowers the uncertainties in the image. Flat frames were also taken, which removes noise from imperfections in the telescope and detector, as well as noise caused by bad pixels. These flat frames depend on the filter used, so a master flat was created for each filter, by firstly subtracting the master bias from each frame, then by taking the median value for each set of flats and finally by normalising each master flat around 1. During the flat combination a sigma-clipping algorithm was again used to discard outlying values. The science images were then corrected by subtracting the master bias frame, and then dividing each science image by the master flat corresponding to the filter used in that science image. Before processing all science and calibration files were cropped to remove the prescan region. This was done using AstroPy (Astropy Collaboration et al., 2013, Price-Whelan et al., 2018) and the CCDPROC package (Craig et al., 2017). The images were corrected using the gain value in the header to get a true electron count, and the errors were propagated as

$$u_{ij} = (g \times p_{ij} + \sigma_{rn}^2)^{0.5} \quad (4)$$

where u_{ij} is the uncertainty in the pixel at (i, j) with value p_{ij} , and the image has gain g and readnoise σ_{rn} .

I then used an implementation of the L.A. Cosmic algorithm (Van Dokkum, 2001) to identify and remove cosmic rays from the science images. The next step was to use the photutils package (Bradley et al., 2019) to identify stars in the image, and then pass the list of stars to the Astrometry.net service (Lang et al., 2010) using the astroquery package (Ginsburg et al., 2013). This was done to accurately plate solve the image, so that each pixel corresponded to a RA/Dec coordinate. The frames for each filter were generally already reasonably aligned, due to the use of guiding during the imaging process, but they were precisely aligned using the astroalign package (Beroiz et al., 2019), which aligns images by matching triangles in each image and determining transformations. This method of alignment was found to be more precise than aligning using the WCS headers on each image, even after plate-solving each image.

The images for each filter were then combined by taking the median value for each pixel to create a master image for each filter, while sigma clipping outliers which were more than 5σ from the median. The uncertainties in each pixel were reduced with the error propagation rule for the statistical median. Currently the counts in each pixel of the images are just the number of photons that were allowed through the filter during the exposure. This will depend on the atmospheric conditions, transmissions of the filter and lenses and the efficiency of the CCD and the specific telescope used. The exact counts will also be distorted by the gain, bias and readout noise of the CCD, although this has now mostly been accounted for. The narrowband images must be transformed from these raw counts, to an absolute flux density so they can be compared to other results. The first step is to correct each image for any difference in exposure time, by dividing out by the exposure time to get a counts per second image. Generally one of the next steps would be to correct for interstellar extinction. However due to the location of NGC 6210, around 1kpc from the galactic plane, Pottasch, S. R. et al., 2009 suggests that this extinction is minimal and a significant correction is not necessary.

The errors were suitably reduced when the images were combined using error propagation rules, and the same transform were applied to each image and error array, to ensure the errors matched up when the images were aligned using astroalign (Beroiz et al., 2019).

3.1.1 Density Determination

The electron density is determined by a ratio of the two sulphur lines in the doublet, so the exact flux calibration is not necessary. As the sulphur lines are close together, it is likely that the continuum contribution will be very similar in both images. The data was also taken at the same time in similar conditions (same airmass), so it is likely that the constant of proportionality between the counts in the flux will be very similar for both cases, and will cancel out in the ratio. The images were also both taken with the same exposure time, 300 seconds, and 5 images were averaged for each filter, meaning they will have a similar uncertainty.

The relation between the SII ratio and density, shown in Figure 2, can be used to determine the density from the ratio of the SII doublet. It was decided that if there are less than 30 counts in a pixel in either image, then a ratio would be meaningless and error-dominated, so in these cases the ratio was set to the unphysical value of 0 to indicate this. As the relation between the ratio and density from Osterbrock and

Ferland, 2006 was in the form of a graph, rather than an empirical formula, the data was extracted using a tool called WebPlotDigitiser (<https://apps.automeris.io/wpd/>) and then interpolated in Python to provide a conversion from ratio to density. Every non-zero pixel in the ratio image of the nebula was then averaged and then uncertainty propagated as the error in the statistical mean to produce an average ratio for the nebula. This average ratio for the nebula was then converted to a density using the interpolation of the ratio-density relation, along with an associated uncertainty.

In addition to this, the density relation was applied on a per pixel scale to generate a 2D map of the nebula density. This provides more insight into density variations inside the nebula, but there is more variation caused by small ratio uncertainties becoming much larger when propagated into a density.

3.1.2 Absolute Flux Calibration

To determine an absolute flux density, in $\text{erg cm}^{-2} \text{ s}^{-1}$, the data needs to be calibrated. This means that for H α and H β lines an absolute flux calibration is needed. This process is taken from Knigge, 2019, but it is summarised here for convenience as it has been modified slightly for use with a extended source like a planetary nebulae. The process requires data of the target in the emission line filter, continuum filter and an overlapping broadband filter. The broadband filter will have a known photometric zero-point (f_0), which is the flux density of a constant source which has a magnitude of 0 in that band. The counts in each filter of a reference star with a known broad-band magnitude ($m_{R,B}$) are used to calibrate the total flux.

The first step is to estimate the number of counts in the emission line filter which aren't due to the line, which is done using the number of counts of the target in the continuum filter multiplied by ratio of the counts of the reference star in the line and continuum filters, which is the same ratio the target would be expected to have if there was no line emission. The difference between the total number of counts of the target in the line and the estimate of the number not due to the line will be the number of counts entirely due to the line emission. This count must then be converted into a flux, using the relationship $f = f_0 \times 10^{m_{R,B}/-2.5}$ where $m_{R,B}$ is the magnitude, f_0 is the zero-point of the filter and f is the flux density. As this flux density is constant across the narrowband filter, we can find the total flux of the reference star from the flux density multiplied by the width of the filter. This flux is proportional to the number of counts of the reference star in the line filter, and so the ratio of these is the needed constant of proportionality that will be true for all the objects in the image. Putting this together we can see the expression for the flux from the line in Equation 5 below, where the subscripts R and T stand for reference and target respectively, and the subscripts C and L stand for continuum and line.

$$F_{T,PL} = (f_0 \Delta \lambda_L) \left(10^{(m_{R,B}/-2.5)} \right) \left[\frac{N_{T,L} - N_{T,C} (N_{R,L}/N_{R,C})}{N_{R,L}} \right] \quad (5)$$

For a point source, with ideal seeing, all the flux would be contained within one pixel, and there would be no need to sum the counts using a virtual aperture. However due to the affects of the atmosphere, and indeed gas/dust between the telescope and the object, the light from the point object will be spread out over more pixels, which is represented by the point-spread function of the object. However for a extended object, like a nebulae, it is possible to either use a very large aperture, and treat the object like a very extended point source in order to get a single estimate of the total flux of the nebula, or to apply the correction per pixel, in order to preserve the spatial distribution of the flux. This allows the production of a 2D image of the nebula in terms of absolute flux, which can then be summed using a virtual aperture to produce the exact same total nebula flux. It is an extra step in the processing but it provides more insight in the spatial variation of the nebula flux. This means that in the calibration above, the counts with subscript R (reference) refer to the total count of a small aperture centred on the reference star, to account for the point spread function, and the counts with subscript T (target) are individual pixel counts.

For the reference star Gaia DR2 1299564611652024064 was selected. It is at RA(2000) $16^h 44^m 21^s$ and Dec(2000) $+23^\circ 47' 30''$. It was located in all the images and a synthetic aperture of radius 5 pixels was used to determine the total number of counts from the star in each filter, using the Python module photutils (Bradley et al. 2019). According to the 2015 APOP catalogue (Qi et al., 2015), this target has has blue (400-500nm) magnitude of 15.967 mag, and a red (600-750nm) magnitude of 14.919. The wavelengths of these measurements does not precisely match the wavelengths of the IAC-80 B and R filters, so an extra

uncertainty in the flux has been estimated at 10%. The photometric zero point of the red (R) filter using the Vega system, is $2.3179 \times 10^{-9} \text{ erg cm}^{-2} \text{ s}^{-1} \text{\AA}^{-1}$, and the photometric zero point of the blue (B) filter is $6.327 \times 10^{-9} \text{ erg cm}^{-2} \text{ s}^{-1} \text{\AA}^{-1}$ (Rodrigo, 2020). The equivalent width of the H α filter is 48.76Å, and the equivalent width of the H β filter is 27.70Å.

The error propagation for this flux calibration is quite complex. There are no uncertainties available for the photometric zero-points or magnitudes of the reference star other than the 10% assumed for the discrepancy in the allowed wavelength of the different filters. Equation 6 shows the total relative error in the flux calibration.

$$\frac{\Delta F}{F} = \sqrt{\left(\frac{N_{T,L}}{N_{R,L}} \sqrt{\left(\frac{\Delta N_{T,L}}{N_{T,L}} \right)^2 + \left(\frac{\Delta N_{R,L}}{N_{R,L}} \right)^2} \right)^2 + \left(\frac{N_{T,C}}{N_{R,C}} \sqrt{\left(\frac{\Delta N_{T,C}}{N_{T,C}} \right)^2 + \left(\frac{\Delta N_{R,C}}{N_{R,C}} \right)^2} \right)^2} \quad (6)$$

where N is the number of counts in the filter, denoted with subscript, C, L, B (continuum, line broadband) of either the target (T) or reference star (R). The ΔN quantities are the errors on the respective counts. For the reference counts, they are the propagated error over the aperture (using 7), and for the target they are the errors on the individual pixel counts that have been propagated through the data reduction. A virtual aperture was then used to sum all the flux from the nebula, in order to determine the total nebula flux density. The aperture used can be seen in Figure 3. The error propagation for the sum over the aperture S_A is

$$\Delta S_A = \sqrt{\sum_{i \in A} \Delta_i^2} \quad (7)$$

where Δ_i is the uncertainty of a pixel in the aperture, summed over the entire aperture A.

The absolute flux calibration works if there is continuum data, but for the H β continuum, which was supposed to be estimated using the H β red filter, the continuum data is unsuitable to be used. The H β red filter, which is centred on 493.4 nm with a width of 4.3nm, is on top of an OIII line, at 493.2nm. This means that the data collected for the continuum in this filter is instead dominated by OIII emission, which comparison of the counts in both images show, as they are generally similar, whereas the expectation would be that the H β emission is several orders of magnitude greater than the continuum. There is a method to instead estimate the continuum emission from the broadband emission, but it will not be as accurate as the broadband emission will also contain emission from the allowed lines within it. The method is again adapted from Knigge, 2019. Equation 5 can be adapted for this case. The only term that refers to the continuum emission at all is $N_{T,L} - N_{T,C}(N_{R,L}/N_{R,C})$. The term that needs to be replaced estimates the number of counts in the line filter that are not from the line emission. The total counts in the broadband filter is the sum of counts from both continuum and line emission. Then the ratio of continuum counts in the broadband and continuum filters will simply be equal to the ratio of the widths of the filters, which is also the ratio that is equal to the counts of the reference star in both filters. Putting it together, the expression for the flux from the line only, $F_{T,PL}$ is given by

$$F_{T,PL} = (f_0 \Delta \lambda_L) \left(10^{(m_{R,B} / -2.5)} \right) \left[\frac{\frac{N_{T,L} - N_{T,B}(N_{R,L}/N_{R,B})}{1 - (N_{R,L}/N_{R,B})}}{N_{R,L}} \right] \quad (8)$$

where the quantities are as they are in Equation 5, with the addition of $N_{T,B}$ which refers to the number of counts of the target in the broadband filter. The error propagation for this calibration was done in the same manner, with the error being the square root of the sum in quadrature of the partial derivative with respect to each term multiplied by the uncertainty in that term. I.e generally

$$\Delta_F = \sqrt{\sum_i \left(\frac{dF}{di} \right)^2 \Delta_i^2} \quad (9)$$

where F is a function of (A, B, C... i), and Δ_i is the uncertainty in the i^{th} variable. Using the now calibrated estimate for the absolute flux of the nebula in the H α and H β , the mean density estimate $\langle n_e \rangle$ from the

forbidden SII doublet, and using the distance estimate from Bohigas et al., 2014 the mass of the ionised hydrogen can be estimated. The total ionised hydrogen mass can be found from Equation 3. All the necessary values have been determined experimentally or been referenced from literature. The error in the mass Δ_M is then given by

$$\Delta_M = M \times \sqrt{\left(\frac{\Delta_{FH\beta}}{F_{H\beta}}\right)^2 + \left(\frac{\Delta_{n_e}}{\langle n_e \rangle}\right)^2 + \left(\frac{2 \times \Delta_D}{D}\right)^2} \quad (10)$$

where $\Delta_{FH\beta}$ is the error in the $H\beta$ flux, Δ_{n_e} is the error in the mean electron density, and Δ_D is the error in the distance. It can be seen that an error in the distance will have a greater effect on the error in the mass due to the fact the distance is being squared.

4 Results and Discussion

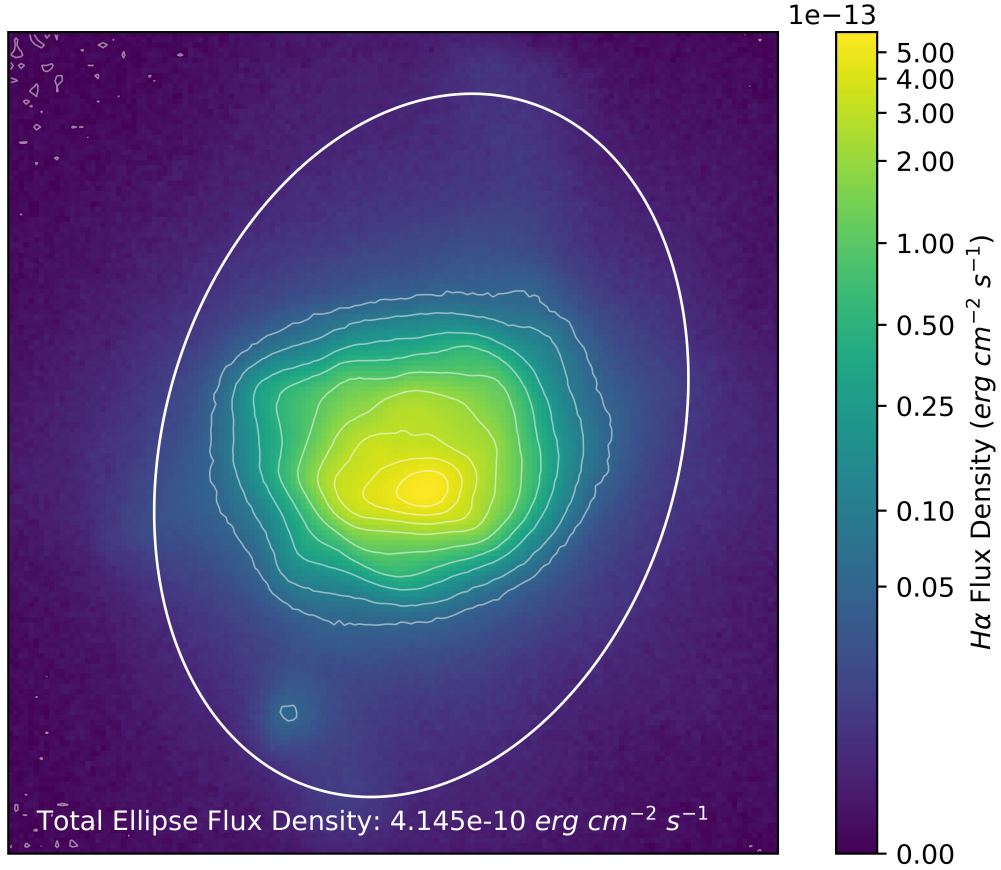


Figure 3: Figure showing the $H\alpha$ flux density of NGC 6210, with an ellipse showing the area of the virtual aperture used to find the total flux density. The levels of the contours are marked on the colorbar.

Figure 3 shows the absolute flux calibration of the $H\alpha$ filter, with contours and the virtual aperture used to sum the counts overlaid. The total $H\alpha$ flux was determined to be $(4.14 \pm 0.01) \times 10^{-10} \text{ erg cm}^{-2} \text{s}^{-1}$. The error in each pixel was propagated through the sum over the whole aperture as shown in Equation 7.

Figure 4 shows the absolute flux calibration of the $H\beta$ filter, with contours and the virtual aperture used to sum the counts overlaid. The total $H\beta$ flux was determined to be $(1.14 \pm 0.03) \times 10^{-10} \text{ erg cm}^{-2} \text{s}^{-1}$. The $H\beta$ flux from Pottasch, S. R. et al., 2009 is given as $1.1 \times 10^{-10} \text{ erg cm}^{-2} \text{s}^{-1}$. No error was provided by the authors, but the result here is identical to two significant figures so I conclude it is equivalent. The relative error on the $H\beta$ is larger than that of $H\alpha$ due to the uncertainty introduced by estimating the continuum from the broadband data.

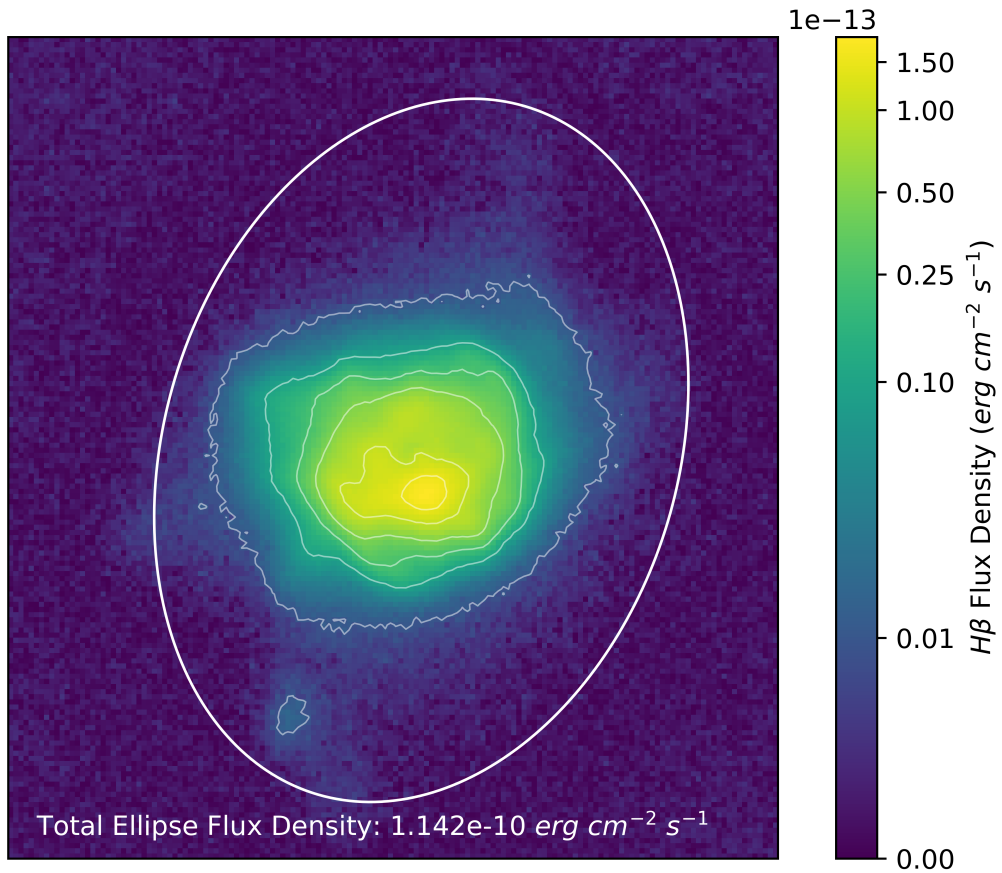


Figure 4: Figure showing the $H\beta$ flux density of NGC 6210, with an ellipse showing the area of the virtual aperture used to find the total flux density. The levels of the contours are marked on the colorbar.

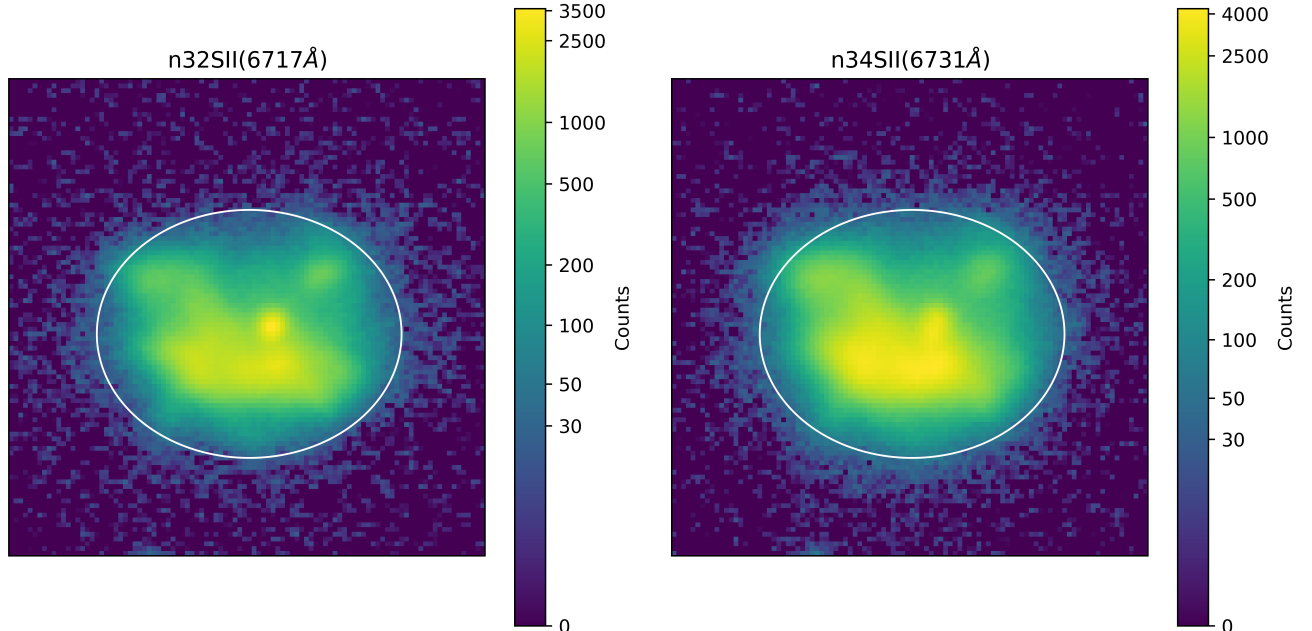


Figure 5: Figure showing the SII doublet (6717\AA and 6731\AA) counts over 300 seconds at a log scale.

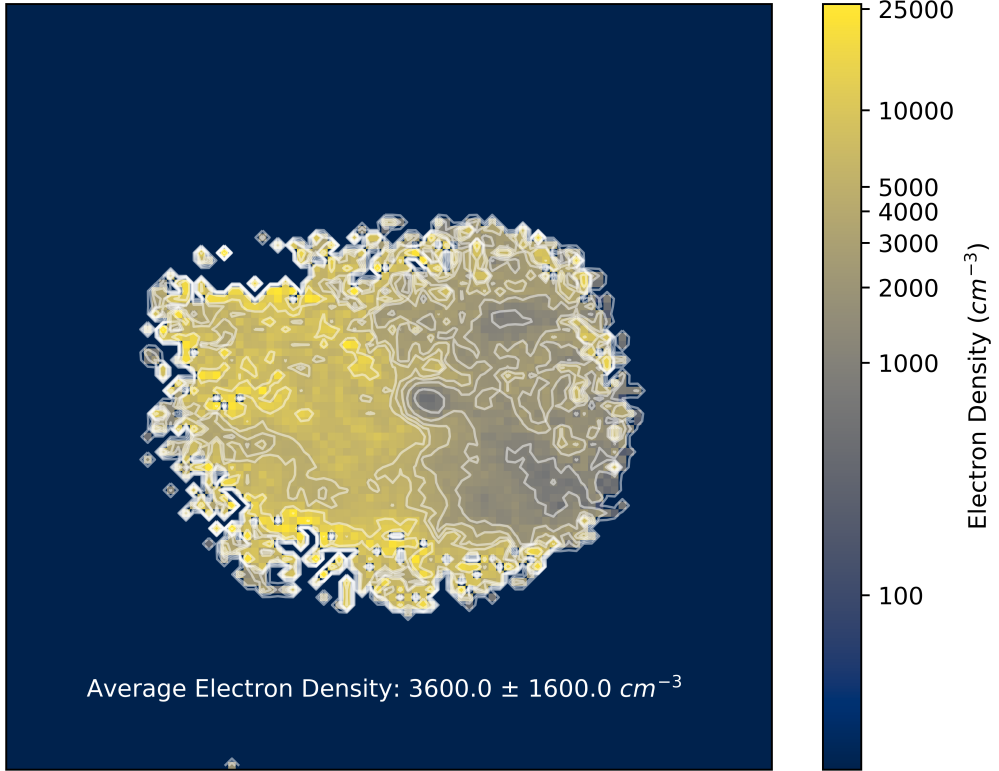


Figure 6: Figure showing the electron density map for NGC 6210 at a log scale. The contour levels are marked on the colorbar.

Figure 5 shows the counts in the forbidden SII doublet. As detailed above, a ratio between this was taken and converted to an electron density using the relation in Figure 2. Figure 6 shows the 2D map of the nebula as a function of electron density. Only the core of the nebula, which is much brighter than the lobes visible in some of the raw images, provided enough counts to make a sensible ratio. The central star is clearly visible in the image as the nearly central point of circular contouring. Some of the denser parts of the nebula, especially the ones near the edge with low counts (as can be seen in Figure 5) have significant error and the actual densities are likely to be much lower. The average electron density, determined from the average of all the pixels in the nebula which passed the criteria set out above (counts/second above 30 in both bands), was found to be $3600 \pm 1600 \text{ cm}^{-3}$. The large uncertainty comes from the increase in uncertainty when taking a ratio, and the propagation of the uncertainty through the conversion to density, where small uncertainties in the ratio propagate into much larger uncertainties in the density. This value is comparable to those found in literature, with Pottasch, S. R. et al., 2009 giving a value of $3000\text{-}4000 \text{ cm}^{-3}$ with a 30% error, and Bohigas et al., 2014 giving a value of 3134^{+4762}_{-1499} for the electron density derived from the [SII] doublet. The value derived here is well within the margin of uncertainty of both of those results. The measurements from those two studies were produced using spectrometers to directly compare line strengths, so it is encouraging that this report has reproduced those results with a more accessible technique.

Using the derived value of the $\text{H}\beta$ flux $F_{\text{H}\beta}$ of $1.13 \times 10^{-10} \text{ erg cm}^{-2} \text{s}^{-1}$, and the value of the mean electron density $\langle n_e \rangle$ of $3600 \pm 1600 \text{ cm}^{-3}$, it is possible to use Equation 10 to estimate a value for the ionised mass of the nebula. The distance was taken from Stanghellini et al., 2008 as $1.57 \pm 0.40 \text{ kpc}$. This gives a nebular mass of $0.071 \pm 0.047 M_\odot$. The relatively high uncertainty (65%) is due primarily to the error in the distance, as the distance is squared in the calculation. The other major contributing factor is the uncertainty in the nebula density. The relative uncertainty in the $\text{H}\beta$ flux is small compared to the other sources of uncertainty.

The value for ionised nebula mass in Bohigas et al., 2014 was given as $0.07 M_\odot$, which is very close to

the value derived in this paper. The authors do not provide an uncertainty on this number. Older sources such as Pottasch, 1980 give slightly higher masses of $0.14 M_{\odot}$ but the more contemporary results have much smaller uncertainties. This nebula mass is quite small when compared to other planetary nebulae. The derivation of the mass equation assumes uniform density and emission throughout the nebula - if there is significant jet emission or non-uniformity that is not along the line of sight, this could account for the lower than theorised mass. The mass of the progenitor is determined in Bohigas et al., 2014 to be $1.2 - 2 M_{\odot}$. Villaver et al. 2002 suggests that the mass of a planetary nebula is expected to be in the order of magnitude of the progenitor star, if not greater, due to the collection of mass from the interstellar medium. The authors go on to suggest the ionised mass estimates often underestimate the total mass because much of it is contained in low density, low surface brightness halos that surround the planetary nebulae. It seems likely that that is true in the case of NGC6210.

The uncertainties in the mass could be reduced with a more accurate estimation of the nebula density, which would require a longer observation time for the forbidden SII doublet. This would also allow analysis of the lobes of the nebula, which with the current data are too faint to be easily analysed. It would also be useful to collect H β continuum data using a different filter, so it would not have to be estimated using the broadband filter. This would allow for a more accurate determination of the H β flux density. Furthermore, collecting narrowband data using an [OIII] and [OII] filters, which would provide a more sensitive temperature metric and a comparison for the SII ratio derived temp respectively.

It is also possible to independently verify the assumed temperature of 9500K using a ratio of the H α and H β lines, but it is a very weak relation which requires precise data to use accurately. The ratio between the H α and H β lines has to be calibrated very precisely, as the ratio must be between 2.825 and 3 to produce a valid nebula temperature. The ratio of H α to H β from the calibrated flux density for this data is 3.63, which is likely due to an overestimation of the H α flux density, as the H β flux matches results from the literature, but I have been unable to find a comparison for H α in the literature. For the assumed temperature of 9500K, the predicted flux density ratio between H α and H β is 2.87. The temperature could also be derived from the [OIII] and [NII] doublets, if data was taken using the appropriate filters, as they are much more sensitive to temperature variation.

5 Conclusion

In this paper I have used narrowband images of the planetary nebula NGC 6210, taken with the IAC-80 in April 2019, to determine line flux densities for emission lines such as H α and H β , as well as measuring ratios of forbidden doublets such as [SII]. I determined an H α flux density of $(4.14 \pm 0.01) \times 10^{-10} \text{ erg cm}^{-2} \text{s}^{-1}$ and a H β flux density of $(1.14 \pm 0.03) \times 10^{-10} \text{ erg cm}^{-2} \text{s}^{-1}$. The H β I have used the [SII] doublet ratio to determine an average electron density of $3600 \pm 1600 \text{ cm}^{-3}$ for the nebula, and also to construct a contour map showing density variation. The calibration of the H β and H α lines using known reference stars and complementary continuum and broadband data, demonstrates the possibility of determining line strengths when a spectrometer is not available.

I used the estimates of the H β flux density and average electron density to estimate the ionised mass of the nebula, which was found to be $0.071 \pm 0.047 M_{\odot}$. This is formally consistent with the value of $0.07 M_{\odot}$ given in Bohigas et al., 2014. However this mass is low given the predicted mass of the progenitor star, and the actual nebula mass is predicted to be higher, with a significant proportion contained in a low density, low surface brightness halo around the planetary nebula.

References

- Astropy Collaboration, Robitaille, T. P., Tollerud, E. J., Greenfield, P., Droettboom, M., Bray, E., Aldcroft, T., Davis, M., Ginsburg, A., Price-Whelan, A. M., Kerzendorf, W. E., Conley, A., Crighton, N., Barbary, K., Muna, D., Ferguson, H., Grollier, F., Parikh, M. M., Nair, P. H., Unther, H. M., Deil, C., Woillez, J., Conseil, S., Kramer, R., Turner, J. E. H., Singer, L., Fox, R., Weaver, B. A., Zabalza, V., Edwards, Z. I., Azalee Bostroem, K., Burke, D. J., Casey, A. R., Crawford, S. M., Dencheva, N., Ely, J., Jenness, T.,

- Labrie, K., Lim, P. L., Pierfederici, F., Pontzen, A., Ptak, A., Refsdal, B., Servillat, M., and Streicher, O. (2013). Astropy: A community Python package for astronomy. , 558:A33.
- Beroiz, M., Cabral, J. B., and Sanchez, B. (2019). Astroalign: A python module for astronomical image registration. *arXiv preprint arXiv:1909.02946*.
- Bohigas, J., Escalante, V., Rodríguez, M., and Dufour, R. J. (2014). Echelle spectroscopy and photoionization modelling of the entire planetary nebula NGC 6210. *Monthly Notices of the Royal Astronomical Society*, 447(1):817–835.
- Bradley, L., Sipőcz, B., Robitaille, T., Tollerud, E., Vinícius, Z., Deil, C., Barbary, K., Günther, H. M., Cara, M., Busko, I., Conseil, S., Droettboom, M., Bostroem, A., Bray, E. M., Bratholm, L. A., Wilson, T., Craig, M., Barentsen, G., Pascual, S., Donath, A., Greco, J., Perren, G., Lim, P. L., and Kerzendorf, W. (2019). astropy/photutils: v0.6.
- Craig, M., Crawford, S., Seifert, M., Robitaille, T., Sipőcz, B., Walawender, J., Vinícius, Z., Ninan, J. P., Droettboom, M., Youn, J., Tollerud, E., Bray, E., Walker, N., Janga, V. R., Stotts, C., Günther, H. M., Rol, E., Bach, Y. P., Bradley, L., Deil, C., Price-Whelan, A., Barbary, K., Horton, A., Schoenell, W., Heidt, N., Gasdia, F., Nelson, S., and Streicher, O. (2017). astropy/ccdproc: v1.3.0.post1.
- Gaia Collaboration (2018). VizieR Online Data Catalog: Gaia DR2 (Gaia Collaboration, 2018). *VizieR Online Data Catalog*, page I/345.
- Ginsburg, A., Robitaille, T., Parikh, M., Deil, C., Mirocha, J., Woillez, J., Svoboda, B., Willett, K., T Allen, J., Grollier, F., and et al. (2013). Astroquery v0.1.
- Irwin, J. (2007). *Astrophysics: Decoding the Cosmos*. Wiley.
- Knigge, C. (2019). Photometry and Line Fluxes. *Physics and Astronomy*.
- Lang, D., Hogg, D. W., Mierle, K., Blanton, M., and Roweis, S. (2010). Astrometry.net: Blind Astrometric Calibration of Arbitrary Astronomical Images. , 139(5):1782–1800.
- Nishiyama, J. J. (2018). *An Introduction to Planetary Nebulae*. 2053-2571. Morgan & Claypool Publishers.
- Osterbrock, D. and Ferland, G. (2006). *Astrophysics Of Gas Nebulae and Active Galactic Nuclei*. University Science Books.
- Pottasch, S. R. (1980). Masses of planetary nebulae. , 89:336–341.
- Pottasch, S. R. (1984). A study of late stages of stellar evolution. *Astrophysics and Space Science Library*, 107.
- Pottasch, S. R., Bernard-Salas, J., and Roellig, T. L. (2009). Abundances in the planetary nebula ngc 6210*. *A&A*, 499(1):249–256.
- Price-Whelan, A. M., Sipőcz, B. M., Günther, H. M., Lim, P. L., Crawford, S. M., Conseil, S., Shupe, D. L., Craig, M. W., Dencheva, N., Ginsburg, A., VanderPlas, J. T., Bradley, L. D., Pérez-Suárez, D., de Val-Borro, M., Paper Contributors, P., Aldcroft, T. L., Cruz, K. L., Robitaille, T. P., Tollerud, E. J., Coordination Committee, A., Ardelean, C., Babej, T., Bach, Y. P., Bachetti, M., Bakanov, A. V., Bamford, S. P., Barentsen, G., Barmby, P., Baumbach, A., Berry, K. L., Biscani, F., Boquien, M., Bostroem, K. A., Bouma, L. G., Brammer, G. B., Bray, E. M., Breytenbach, H., Buddelmeijer, H., Burke, D. J., Calderone, G., Cano Rodríguez, J. L., Cara, M., Cardoso, J. V. M., Cheedella, S., Copin, Y., Corrales, L., Crichton, D., D’Avella, D., Deil, C., Depagne, É., Dietrich, J. P., Donath, A., Droettboom, M., Earl, N., Erben, T., Fabbro, S., Ferreira, L. A., Finethy, T., Fox, R. T., Garrison, L. H., Gibbons, S. L. J., Goldstein, D. A., Gommers, R., Greco, J. P., Greenfield, P., Groener, A. M., Grollier, F., Hagen, A., Hirst, P., Homeier, D., Horton, A. J., Hosseinzadeh, G., Hu, L., Hunkeler, J. S., Ivezić, Ž., Jain, A., Jenness, T., Kanarek, G., Kendrew, S., Kern, N. S., Kerzendorf, W. E., Khvalko, A., King, J., Kirkby, D., Kulkarni, A. M.,

- Kumar, A., Lee, A., Lenz, D., Littlefair, S. P., Ma, Z., Macleod, D. M., Mastropietro, M., McCully, C., Montagnac, S., Morris, B. M., Mueller, M., Mumford, S. J., Muna, D., Murphy, N. A., Nelson, S., Nguyen, G. H., Ninan, J. P., Nöthe, M., Ogaz, S., Oh, S., Parejko, J. K., Parley, N., Pascual, S., Patil, R., Patil, A. A., Plunkett, A. L., Prochaska, J. X., Rastogi, T., Reddy Janga, V., Sabater, J., Sakurikar, P., Seifert, M., Sherbert, L. E., Sherwood-Taylor, H., Shih, A. Y., Sick, J., Silbiger, M. T., Singanamalla, S., Singer, L. P., Sladen, P. H., Sooley, K. A., Sornarajah, S., Streicher, O., Teuben, P., Thomas, S. W., Tremblay, G. R., Turner, J. E. H., Terrón, V., van Kerwijk, M. H., de la Vega, A., Watkins, L. L., Weaver, B. A., Whitmore, J. B., Woillez, J., Zabalza, V., and Contributors, A. (2018). The Astropy Project: Building an Open-science Project and Status of the v2.0 Core Package. , 156:123.
- Qi, Z., Yu, Y., Bucciarelli, B., Lattanzi, M. G., Smart, R. L., Spagna, A., McLean, B. J., Tang, Z., Jones, H. R. A., Morbidelli, R., Nicastro, L., and Vecchiato, A. (2015). Absolute Proper Motions Outside the Plane (APOP)&mdashA Step Toward the GSC2.4. , 150(4):137.
- Rodrigo, C., S. E. B. A. (2020). The svo filter profile service.
- Stanghellini, L., Shaw, R. A., and Villaver, E. (2008). The magellanic cloud calibration of the galactic planetary nebula distance scale. *The Astrophysical Journal*, 689(1):194–202.
- Van Dokkum, P. G. (2001). Cosmic-ray rejection by laplacian edge detection. *Publications of the Astronomical Society of the Pacific*, 113(789):1420.
- Villaver, E., Manchado, A., and Garcia-Segura, G. (2002). The dynamical evolution of the circumstellar gas around low- and intermediate-mass stars. II. the planetary nebula formation. *The Astrophysical Journal*, 581(2):1204–1224.